Liquid Crystals
Publication details, including instructions for authors and subscription information:
http://www.informaworld.com/smpp/title~content=t713926090

Nematicons: self-localised beams in nematic liquid crystals

Gaetano Assanto[a]; Mirosław A. Karpierz[b]
[a] NooEL, Nonlinear Optics and OptoElectronics Lab, University "Roma Tre", Rome, Italy [b] Faculty of Physics, Warsaw University of Technology, Warsaw, Poland

Online publication date: 18 November 2009

To cite this Article Assanto, Gaetano and Karpierz, Mirosław A.(2009) 'Nematicons: self-localised beams in nematic liquid crystals', Liquid Crystals, 36: 10, 1161 — 1172
To link to this Article: DOI: 10.1080/02678290903033441
URL: http://dx.doi.org/10.1080/02678290903033441

Liquid Crystals,
Vol. 36, Nos. 10–11, October–November 2009, 1161–1172

Taylor & Francis
Taylor & Francis Group

INVITED ARTICLE

Nematicons: self-localised beams in nematic liquid crystals

Gaetano Assanto[a]* and Mirosław A. Karpierz[b]

[a]*NooEL, Nonlinear Optics and OptoElectronics Lab, University "Roma Tre", Via della Vasca Navale 84, 00146 Rome, Italy*
[b]*Faculty of Physics, Warsaw University of Technology, Koszykowa 75, 00662 Warsaw, Poland*

(Received 21 April 2009; final form 11 May 2009)

We review the impressive progress on light self-localisation into spatial optical solitons in nematic liquid crystals. We summarise the basic physics and models, outlining the main properties of nematicons and providing an overview of the most significant experimental achievements in undoped, planar, twisted and chiral nematic liquid crystals.

Keywords: spatial solitons; reorientational non-linearity; liquid crystals

1. Introduction

Liquid crystals are very attractive for non-linear photonics, particularly in devices for light switching and all-optical circuits. Liquid crystals, in ordered phases such as the nematic one, exhibit a large (optical and radio-frequency) birefringence and their dielectric properties can be modified by external fields as well as by light through a non-linear response (*1–4*). The main contribution to the latter arises from either thermo-optic or reorientational processes. While the thermal effect is analogous to that observed in other dielectric materials in the presence of absorption, the reorientational response is characteristic of liquid crystals with some degree of orientation order. Such non-linearity can induce extremely large changes in refractive index at relatively low light powers, depends on both boundary conditions and geometry of the system and can be easily altered by temperature as well as external electric or magnetic fields. Moreover, light reorientation is polarisation sensitive but substantially independent of wavelength in the whole transparency range, typically from visible to mid-infrared (*1*, *2*). The main drawback of reorientation in liquid crystals is the relatively long response time, as it is determined by molecular motion in a fluid; however, specific optimisation of the structures and applications to readdressable interconnects in reconfigurable circuits are successful routes to overcome this limitation.

The all-optical response in nematic liquid crystals (NLC) supports various phenomena (*2–4*) and, in particular, the formation and propagation of stable and robust self-trapped (non-diffractive) light beams, also known as nematicons (*5*, *6*). While the first evidence of spatial solitary waves (i.e. solitons) was provided in capillaries filled with dye-doped NLC (*7–9*), the most studied geometries rely on planar cells with undoped NLC, various anchoring conditions and applied biases. In the next section we summarise the basic physics underlying the formation of nematicons. In Section 3 we review the main findings on nematicons in undoped liquid crystals, outlining the main achievements in terms of soliton control and interactions. In Section 4 we focus on solitons in twisted and chiral NLC.

2. Optical non-linearity in nematic liquid crystals

Nematic liquid crystals are a family of dielectric media with various mechanisms of optical non-linearity including electronic, thermal, photorefractive or electrostrictive (*1–4*). Their signature, however, is the reorientational non-linearity. The latter is connected with the microscopic structure of NLC, which consists of anisotropic molecules usually with a rod-like (elongated) shape. In the isotropic phase (i.e. when the molecules lack both positional and orientational order) the electric field of a light wave can induce some orientation order in the liquid, modifying the average refractive index. This non-linearity enhances with temperature and is roughly proportional to $(T - T^*)^{-1}$, with $T^* < T_c$ the temperature of the second-order phase transition and T_c the temperature of clearing, according to the theory by de Gennes and Landau (*1*, *2*).

In the nematic liquid-crystalline phase the elastic interaction between the molecules induces orientation ordering but allows the flow of molecules. At a given temperature, NLC molecules fluctuate around a mean direction defined by the unity vector **n** and called *director*. In addition, the anchoring conditions at the

*Corresponding author. Email: assanto@uniroma3.it

ISSN 0267-8292 print/ISSN 1366-5855 online

DOI: 10.1080/02678290903033441
http://www.informaworld.com

boundaries (e.g. surface rubbing) and the effect of elastic intermolecular forces determine the spatial orientation of the NLC in a cell. The changes in director orientation relate to the free energy density:

$$f_F = \frac{1}{2}K_{11}(\nabla\cdot\mathbf{n})^2 + \frac{1}{2}K_{22}(\mathbf{n}\cdot\nabla\times\mathbf{n} + G)^2 + \frac{1}{2}K_{33}(\mathbf{n}\times\nabla\times\mathbf{n})^2 \quad (1)$$

with K_{ii} the elastic constants for the three basic deformations of the molecules: splay ($i = 1$), twist ($i = 2$), and bend ($i = 3$); normally $K_{33} > K_{11} > K_{22}$ and all of them of the order of 10^{-11} N. In standard theoretical analyses the equations can be simplified by assuming that all the elastic constants are equal (single constant approximation). The parameter G in the twist deformation component is responsible for chirality: $G = 0$ for pure NLC and $G = 2\pi/p$ for chiral NLC (ChNLC), with p being the pitch.

Liquid crystalline molecules are elongated and this is responsible for the anisotropic properties of NLC, particularly in terms of electrical permittivity. Thereby, an external electric field **E** can induce a torque that tends to rotate the major molecular axis and align it towards the applied field vector. The interaction energy density connected with orientation changes due to an electric field is

$$f_{el} = -\frac{\varepsilon_0\Delta\varepsilon}{2}\left\langle(\mathbf{n}\cdot\mathbf{E})^2\right\rangle \quad (2)$$

where $\Delta\varepsilon = \varepsilon_{\parallel} - \varepsilon_{\perp}$ is the anisotropy in permittivity, $\varepsilon_{\parallel}$ and $\varepsilon_{\perp}$ are the components of electric permittivity for extraordinary and ordinary polarisations, respectively. For a positive anisotropy $\Delta\varepsilon > 0$ this energy is minimised when the molecules are parallel to the electric fields. Although a similar behaviour takes place for magnetic field, the magnetic anisotropy is usually much lower than the electric one and, at optical frequencies, the interaction between light and NLC is dominated by the electric field.

Molecular orientation in a liquid crystalline cell is the result of the interaction with external fields and boundaries. Since the molecules are non-polar, it does not depend on the sign of the field and occurs for time-varying excitations, as well, including waves at optical frequencies. As the NLC birefringence is connected with the director orientation, changes in the latter also determine the rotation of the optic axis in the equivalent uniaxial crystal. Otherwise stated, light in the extraordinary polarisation, i.e. with **E** vector coplanar but not collinear with the optic axis and the wave vector, can modify the electric permittivity tensor, increase the extraordinary index of refraction and give rise to self-focusing.

To calculate the light-induced reorientation, the free energy needs be minimised. The total free energy density includes deformation energy and the interaction energy with external fields and boundaries. In addition, for a time-dependent analysis it is necessary to introduce the dissipation energy density f_R connected with the orientational viscosity γ. In its simplest form the latter can be expressed as $f_R = \frac{1}{2}\gamma(\partial\mathbf{n}/\partial t)^2$.

The minimisation leads to the Euler–Lagrange–Rayleigh equations. It is convenient to define the orientation angle θ between the director **n** and one of the coordinates. The angle θ suffices to describe the NLC orientation in two-dimensional problems, i.e. when the NLC director at the boundaries and the electric field vector **E** lie in the same plane (e.g. as in the configuration shown in Figure 1). For the geometry sketched in Figure 1 the director $\mathbf{n} = (\sin\theta, 0, \cos\theta)$ and, in the single (elastic) constant approximation (i.e. $K = K_{11} \approx K_{22} \approx K_{33}$), the Euler–Lagrange–Rayleigh equation takes the form

$$\frac{\partial^2\theta}{\partial x^2} + \frac{\partial^2\theta}{\partial z^2} - \frac{\varepsilon_0\Delta\varepsilon}{2K}\left[\left(E_xE_z^* + E_x^*E_z\right)\cos 2\theta + \left(|E_z|^2 - |E_x|^2\right)\sin 2\theta\right] = \frac{\gamma}{K}\frac{\partial\theta}{\partial t} \quad (3)$$

where E_x and E_x are the average electric field components (for monochromatic waves they equal half of the amplitudes). Equation (3) with boundary conditions $\theta(x = -d/2)$ and $\theta(x = d/2)$ describes the NLC orientation in the presence of electric fields at a given frequency and corresponding to an anisotropy $\Delta\varepsilon$. If the director distribution is modified by fields at other frequencies (optical as well as low or constant), then the left-hand side of Equation (3) should contain the superposition of components with the pertinent dielectric anisotropies. Finally, since reorientation affects the optic axis, which is locally parallel to the director **n**, Maxwell's equations in an anisotropic uniaxial need to complete the set of equations describing the evolution of a beam in such a system.

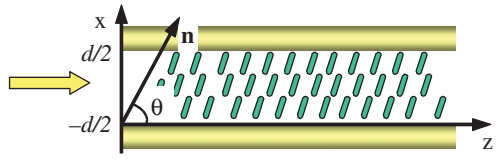

Figure 1. Configuration of a bounded NLC layer for a 2D case (see e.g. (*5*)). The **E**-field lies in the plane xz of the drawing. The arrow represents the input wave vector.

When the applied electric field forms an angle $\pi/2$ with respect to **n**, then the corresponding torque is null below a threshold value known as Freedericksz transition (*2*, *3*). Reorientation can take place above threshold due to angular fluctuations in the molecular director, but it requires rather substantial electric fields. This behaviour is presented in Figure 2, plotting reorientation versus electric field intensity for various initial angles $\theta = \theta_0$: for $\theta_0 = 0$ (solid line) reorientation starts above the threshold intensity. An increase in θ_0 (i.e. reducing the initial angle between **E** and **n**) lowers the intensity required for reorientation as well as the maximum achievable index change.

Molecular reorientation in NLC is a non-local effect: the induced variation in director (i.e. index) distribution is wider that the profile of the applied field. Figure 3 displays the calculated distribution of $\theta(x)$ as compared with a bell-shaped electric field excitation for various intensities I_0. The boundary conditions also affect the non-local response and its strength depending on the transverse size (waist) of the beam (*10–12*).

NLC are non-local in space and, therefore, also in time. This is the main drawback of the reorientational non-linearity in NLC, with response times of the order of a hundred milliseconds or larger, this value depending on viscosity, elastic constants, layer thickness and excitation; the calculated dependence on intensity is visible in Figure 4.

In summary, the features of the reorientational response of NLC are unique in many ways and determine their non-linear character and the properties of nematicons. In particular, the non-linearity is polarisation sensitive, self-focusing, saturable and non-local; hence, it can support stable two-dimensional solitons. Due to the actual perturbation in index and the non-local response, changes induced by one beam correspond to the formation of a (channel) waveguide able to confine optical waves of different (even larger) wavelength. Moreover, by tailoring the input beam polarisation and the boundary conditions on the director (determined by anchoring at the surrounding plates and/or by an externally applied voltage bias through proper electrodes), the all-optical response can be maximised and the required input power minimised, thereby drastically reducing or

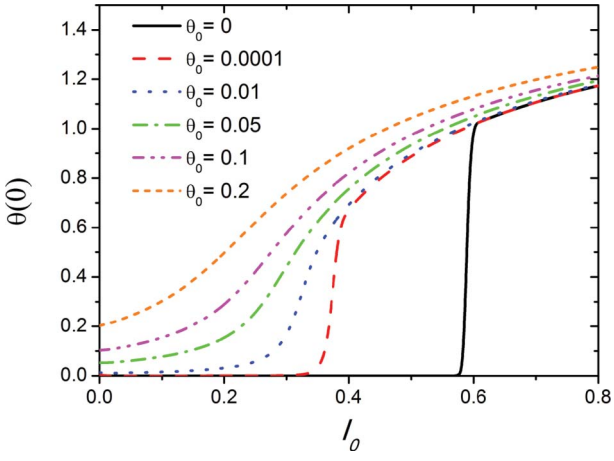

Figure 2. Calculated orientation angle $\theta(0)$ versus electric field intensity for different boundary conditions $\theta(-d/2) = \theta(d/2) = \theta_0$ and an NLC layer thickness $d = 50\mu$m. The electric field employed in the calculations has the form $E_x^2 = I_0(\varepsilon_0\Delta\varepsilon/4Kw^2)[0.01 + 0.1\exp(-x^2/w^2)]$ with $w = 2\ \mu$m.

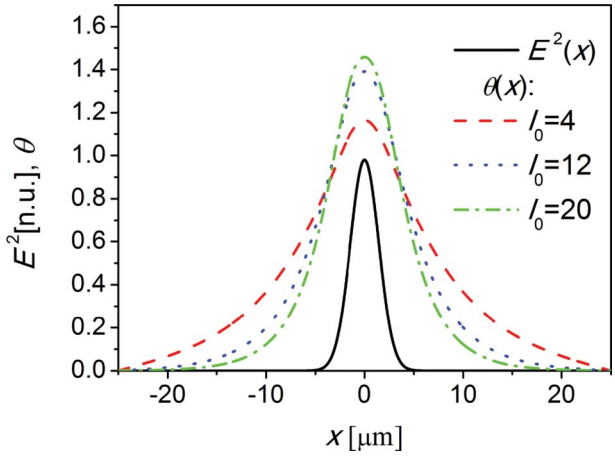

Figure 3. The distribution of $\theta(x)$ for various electric field excitations. The field (solid line) and the layer thickness are as in Figure 2 and the boundary conditions are $\theta(-d/2) = \theta(d/2) = 0.001$.

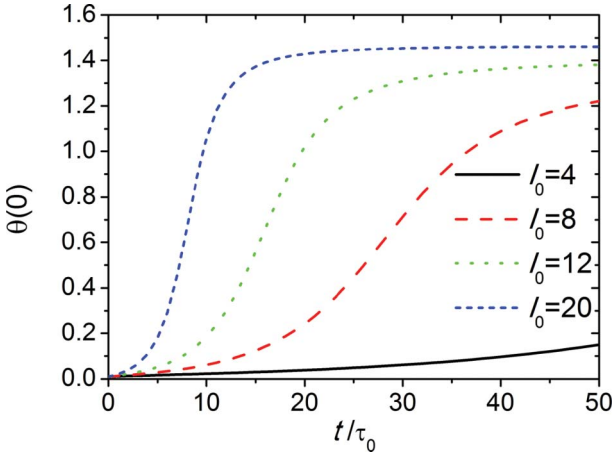

Figure 4. Increase in orientation $\theta(0)$ versus time t/τ_0 for various intensities. The electric field and NLC thickness are as in Figures 2 and 3 and the relaxation time is $\tau_0 = \gamma w^2/4K$

eliminating the occurrence of undesired thermal effects. In the following we will review excitation and properties of low-power reorientational nematicons in threshold-less configurations.

Nematicons have been observed in a number of geometries, the main planar ones being sketched in Figure 5. When the thickness of the cell is much larger than the wavelength and the waist of an input light beam, then the NLC layer can be treated as a bulk and the observation of (2+1) dimensional solitons is possible. Conversely, when the thickness is comparable with the wavelength and the beam size, then a liquid crystalline cell should be treated as a planar waveguide and can support (1+1) dimensional nematicons.

In the homeotropic orientation (Figure 5(a)) the director is perpendicular to the boundaries; electric fields with the only component E_x cannot induce reorientation, whereas $\mathbf{E} = \mathbf{y}E_y$ can reorient the NLC at intensities above the Freedericksz threshold. Stable self-trapped beams in one-transverse dimension (i.e. in planar waveguides) were indeed observed for input polarisations close but not parallel to $\mathbf{E} = \mathbf{x}E_x$ (*13*, *14*). In the planar texture (Figure 5(b)) the director **n** is parallel to the plates yz defining the cell and the threshold exists for the two linear polarisations: $\mathbf{E} = \mathbf{x}E_x$ and $\mathbf{E} = \mathbf{y}E_y$. However, by applying an external (low-frequency or continuous wave) electric field (i.e. a voltage) across the NLC thickness, the molecules can be pre-tilted at some angle $0 < \theta < \pi/2$ in the plane xz, allowing the incoming linearly polarised light to force further reorientation without threshold and create stable nematicons. Similarly, planar anchoring with the director parallel to yz but at an angle $0 < \theta_0 < \pi/2$ can support nematicons excited by $\mathbf{E} = \mathbf{y}E_y$. Nematicons were also observed in planar geometries with director parallel to the boundary plates in yz but twisted within the layer thickness (Figure 5(c)). As a result, the molecular director was neither parallel nor perpendicular to the electric field $\mathbf{E} = \mathbf{y}E_y$ in the whole NLC volume, allowing a low-power self-focusing and the formation of nematicons with non-planar trajectories across the thickness of the non-uniform dielectric distribution. Finally, it is worth mentioning that, in the frame of discrete light propagation, nematicons have also been investigated in one-dimensional arrays of coupled channel waveguides realised in NLC (*15–19*).

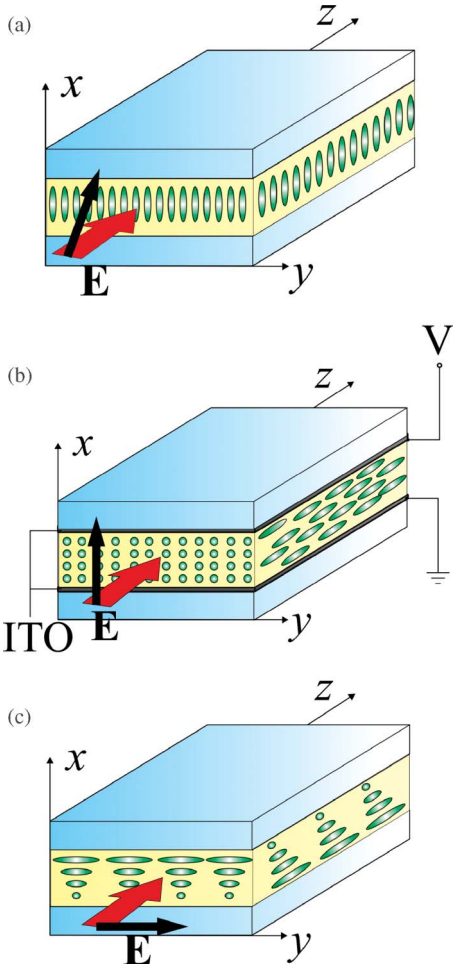

Figure 5. Typical NLC planar configurations for the investigations of optical spatial solitons: (a) homeotropic anchoring; (b) planar anchoring with external voltage bias through Indium Tin Oxide (ITO) thin film electrodes, (c) twisted or chiral arrangement.

3. Spatial solitons in bulk nematic liquid crystals

The simplest geometry initially adopted for demonstrating nematicons in a planar cell filled with undoped NLC (commercial mixture E7) is as illustrated in Figure 1 and Figure 5(b). The input interface prevented the formation of an NLC meniscus and undesired depolarisation on the input beam, the latter linear polarised with the E-field parallel to x. Two indium tin oxide (ITO)-coated glass plates defined upper and lower interfaces to confine the liquid crystals by capillarity, and Mylar spacers ensured a controlled NLC thickness of 75 μm. Rubbed polyimide films provided the anchoring at the boundaries and a low-frequency voltage was applied via the ITO transparent electrodes in order to pre-tilt the director at $\theta \neq 0$ and eliminate the Freedericksz threshold (*1–3*, *19*, *20*).

The boundary-anchored NLC is a positive uniaxial with $n^2(\theta) = \cos^2\theta/n_\perp{}^2 + \sin^2\theta/n_{||}{}^2$ and $n_e < n(\theta(x)) < n_o$, where $n_e = n_{||} = \sqrt{\varepsilon_{//}}$ and $n_o = n_\perp = \sqrt{\varepsilon_\perp}$. In the presence of an externally applied voltage $V = dE_{rf}$, with d the cell thickness, the evolution of the slowly varying

envelope A of a beam linearly polarised along x and propagating along z in the midplane of the cell is governed by (*20*, *21*)

$$2ik\frac{\partial A}{\partial z} + \nabla_{\perp}^2 A + k_0^2(n_{//}^2 - n_{\perp}^2) \left[\sin(\theta)^2 - \sin(\theta_0)^2\right] A = 0,$$

$$K\frac{\partial^2\theta}{\partial z^2} + K\nabla_{\perp}^2\theta + \frac{\Delta\varepsilon_{RF}E_{rf}^2}{2}\sin(2\theta) + \frac{\varepsilon_0(n_{//}^2 - n_{\perp}^2)|A|^2}{4}\sin(2\theta) = 0 \qquad (4)$$

with $k = k_0 n(\theta)$, k_0 the vacuum wavevector, θ_0 the peak pre-tilt of the NLC director in the absence of optical excitation, θ the overall director orientation owing to both light and voltage, $K = K_{11} \approx K_{22} \approx K_{33}$ the Frank's elastic constant and $\Delta\varepsilon_{RF}$ the dielectric anisotropy in the quasi-static limit. The x-symmetric bias-preset orientation $\Theta(x)$ is given by (*2*, *3*)

$$K\frac{d^2\Theta}{dx^2} + {}^1\!/_2\Delta\varepsilon_{RF}E_{rf}^2\sin(2\Theta) = 0.$$

Equation (4), in the limit of a narrow soliton as compared with the cell thickness, can be reduced to a well-conditioned non-linear Schroedinger equation with stable 2D+1 soliton solutions owing to the stabilising non-local response. By linearising the corresponding anharmonic oscillator potential, an (approximate) existence curve of the form $PW_s^2 = P_c R_c^2$ can be obtained for nematicons in this geometry, as plotted in Figure 6, P being the input excitation power, W_s, P_c and R_c reference values for the waist, the critical power and the range of non-locality, respectively (*21*).

The acquired evolution displayed in Figure 7 shows that, indeed, nematicons are breathers with a periodic waist oscillation for any given excitation, such periodicity decreasing at higher powers (*22*). Such behaviour is consistent with the high non-locality characterising liquid crystals, as originally pointed out by Snyder and Mitchell (*23*). In addition, nematicons are extraordinarily polarised wave packets subject to birefringent walk-off

$$\delta(\theta) = \arctan\left(\frac{\left(n_{//}^2 - n_{\perp}^2\right)\sin(2\theta)}{n_{//}^2 + n_{\perp}^2 + \left(n_{//}^2 - n_{\perp}^2\right)\cos(2\theta)}\right),$$

previously neglected in Equation (4); hence, their Poynting vector is non-collinear with the wave vector and solitons excited with wave vector parallel to z tend to move in the plane xz and eventually interact with the boundaries (*10*, *24*). Proper care must therefore be used in launching nematicons in finite-size cells in order to prevent or correct undesired deviations in trajectory and final size at the cell output (*24*), particularly when the solitary waveguide is intended for transmission of a weaker (copolarised) signal (*25*),

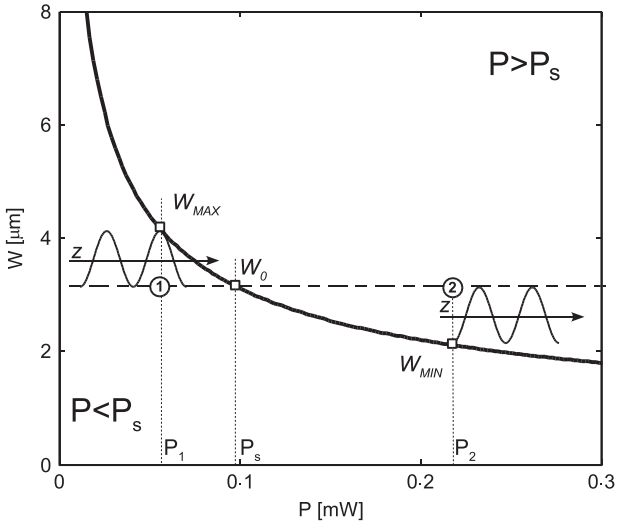

Figure 6. Calculated existence curve of stationary nematicons in E7. Every point in the Waist-Power plane corresponds to a breather waist periodically oscillating between its initial value (W_0) and that corresponding to $P \neq P_s$ on the curve. Pairs W–P on the curve represent invariant solitons, i.e. those with an infinitely long oscillation cycle.

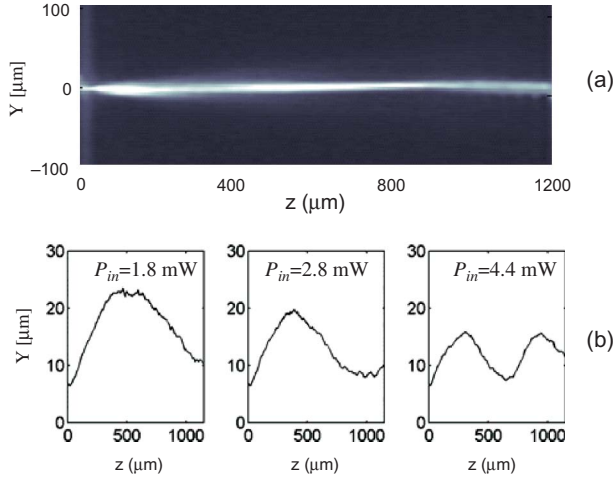

Figure 7. (a) Propagation of a breathing nematicon. (b) Soliton waist versus propagation distance for various input powers P_{in}.

when the excitation power varies and/or the interfaces interact with the self-localised beam (*10*, *22*, *26*, *27*).

Figure 8 displays experimentally acquired examples of nematicons generated by visible light at 514 nm and guiding a probe signal at 632.8 nm. Figure 9 shows linear diffraction (top) and a soliton (bottom) as generated by a spatially incoherent (speckled) input beam and confining a weak probe with similar linear characteristics (*28–30*): clearly the transverse non-locality of NLC acts as a low-pass spatial frequency filter and allows incoherent light to generate solitons at the price of a slightly larger excitation (2.7 > 2.0 mW). Owing to this incoherent feature of the non-local response, vector nematicons encompassing two (or more) wavelengths can also be generated by collinear copolarised beams of comparable powers (*31*, *32*).

The highly non-local character of nematicons (*21*) has important effects on their propagation in the presence of extra nematicons in the same plane (e.g. *yz*) of propagation (*33–35*), when launched in the NLC bulk with an initial angular momentum (*36–38*), when external light beams modify the refractive response of the NLC in the proximity of their trajectory (*39*, *40*). Some in-plane nematicon–nematicon interactions are summarised in Figure 10(a) to (e): mutual attraction is shown in Figure 10 (two (a) or three (b) nematicons) and can be effectively exploited to realise logic gates (*34*). When an intense beam goes through the cell thickness, perpendicular to the plane of soliton propagation, a lens-like perturbation (converging or diverging depending on the polarisation of the **E**-field) can modify the solitary trajectory, as illustrated in Figure 10(c) to (e). The out-of-plane nematicon–nematicon interaction supports power-dependent spiralling of the resulting cluster (*36–38*), as sketched in Figure 11(a) for two nematicons and

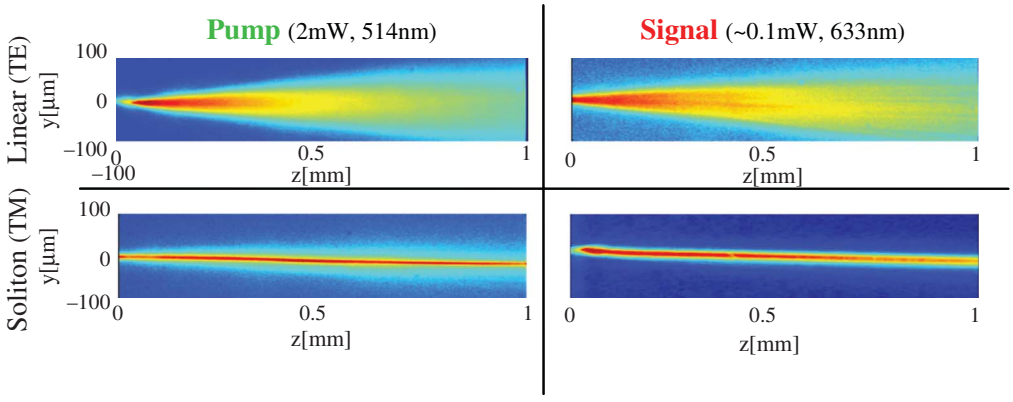

Figure 8. Colour-coded photographs of beam propagation from an Argon laser (left) and a collinear copolarised Helium-Neon laser (right) in an NLC planar cell. Top panels: linear propagation with diffraction when employing an input polarisation orthogonal to the molecular director. Bottom panels: (left) soliton propagation in the extraordinary polarisation (parallel to *xz*) and (right) corresponding confinement of the probe.

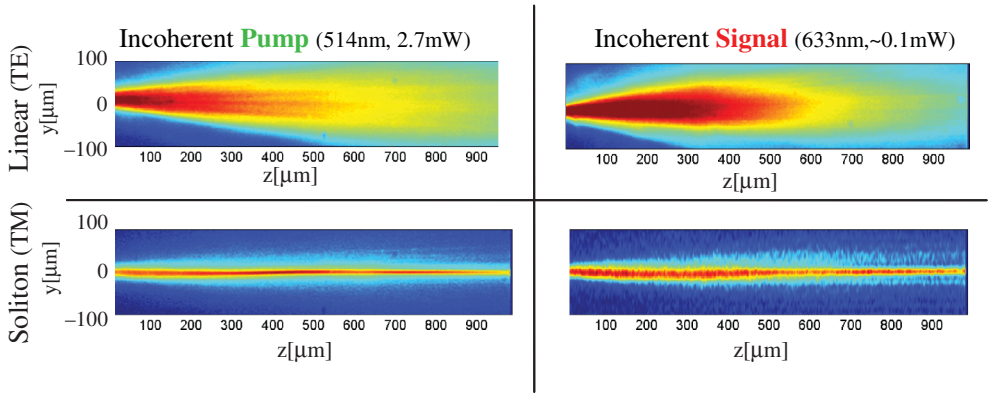

Figure 9. Spatially incoherent (speckled by a diffuser) beam propagation from an Ar+ laser (left) and a collinear copolarised He-Ne laser (right) in a planar cell. Top panels: linear propagation with diffraction when injecting a beam with $\mathbf{E} \perp \mathbf{n}$. Bottom panels: (left) soliton propagation in the extraordinary polarisation ($\mathbf{E} \,//\, xz$) and (right) corresponding confinement of the probe.

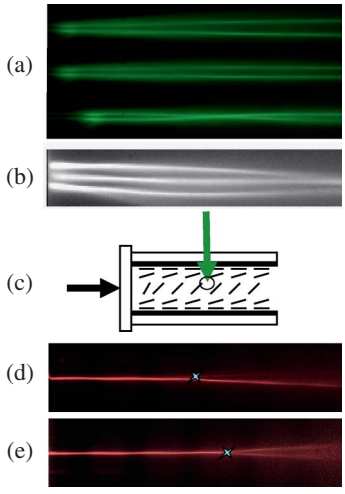

Figure 10. Examples of nematicon trajectories all-optically controlled by (a, b) other in-plane nematicons or an external beam (c) to (e). (a) Two nematicons are launched at a relative angle of 1.7° and tend to propagate independently at low power (top), to mildly attract and propagate parallel to one another (mid-photo) or interleave at high power (bottom). (b) Example of three in-plane nematicons mutually attracting. (c) Sketch of interaction between a nematicon (black arrow) and an external beam (green) in a planar NLC cell; the lens-like (defocusing) perturbation can interact (d) on axis with the soliton, causing its deviation sideways or (e) head-on, causing its splitting. The stars indicate the position of the external beam with respect to the nematicon.

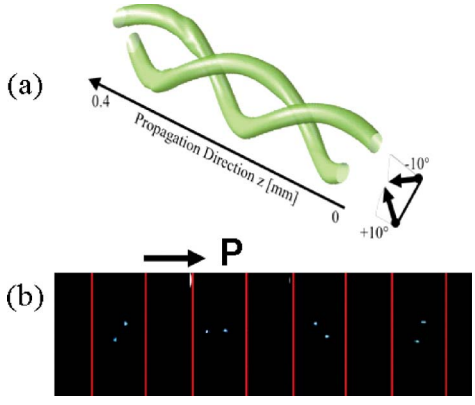

Figure 11. (a) Two nematicon cluster formed by two equi-power out-of-plane extraordinary-polarised beams launched with initial angular momentum. (b) As the input power was increased, the angular speed of the cluster increased, as well, yielding larger rotations after a given propagation distance in the cell, as visible in the photographic sequence.

demonstrated by the photosequence in Figure 11(b) for increasing excitation: the cluster rotation after a finite propagation (i.e. at the cell output) is proportional to the input power (*36*, *37*). Furthermore, more nematicons can be excited by a wider input beam though modulational instability, the latter exhibiting non-local features, as well (*41–44*). Several nematicons in the non-local NLC fluid dielectric can also stem from a dispersive shock wave or undular bore (*45*) and result in a complex behaviour versus propagation (*46*, *47*).

Being stable and robust owing to their non-local character, nematicons can propagate through non-uniform dielectric regions, in analogy to plane waves but retaining their wave-packet nature of transversely self-confined beams. Moreover, since they stem from the NLC reorientational response to extraordinary polarised beams, their energy flux (Poynting vector) is non-collinear with the wave vector and they are subject to a walk-off δ of the order of several degrees due to the large birefringence (e.g. $n_{//} - n_{\perp} \approx 0.2$ in E7). Thereby, since a low frequency bias can alter the extraordinary plane of propagation by reorienting the director **n**, nematicons can be redirected based on the corresponding voltage-driven change in walk-off (*48*, *49*)). Such change can be more easily exploited in cells with molecular director initially lying in the yz plane at a finite angle ($0 < \theta < \pi/2$) with an incoming **E** // ***y***. An image of the trajectory can be acquired with a microscope and a camera: an example of bias-induced angular steering of about 7° is shown in Figure 12 (*48*). A light-induced version of this bias-induced change in director and walk-off was recently demonstrated in a liquid crystal light valve, where external light can effectively change the applied bias with the aid of a photoconductive film at one of the NLC interfaces (*50*).

The basic concept exploited in changing walk-off and trajectory can be extended to define two dielectric regions with separate voltage biases, thereby forming a graded interface through which the nematicon can undergo refraction or even total internal reflection depending on the sign and size of the corresponding changes in θ; i.e., changes in refractive index, director distribution and walk-off. With this approach, refraction as large as –18° and total internal reflection with nematicon deviations of 22° were demonstrated in cells with E7 (*51*, *52*). Moreover, owing to the dependence of the reorientational non-linearity with bias (*53*), huge non-linear lateral beam (Goos-Hänchen type) shifts could be observed when varying the soliton power (*54*). Similar results were also reported using the all-optical response of a dye-doped NLC to external beams defining (double) interfaces for soliton refraction and total internal reflection TIR (*55*), as displayed in Figure 13. It is worth mentioning that, due to the large walk-off stemming from the significant birefringence of NLC, even negative refraction and its tuning to normal (positive) were reported for nematicons travelling through a suitably prepared interface (*56*).

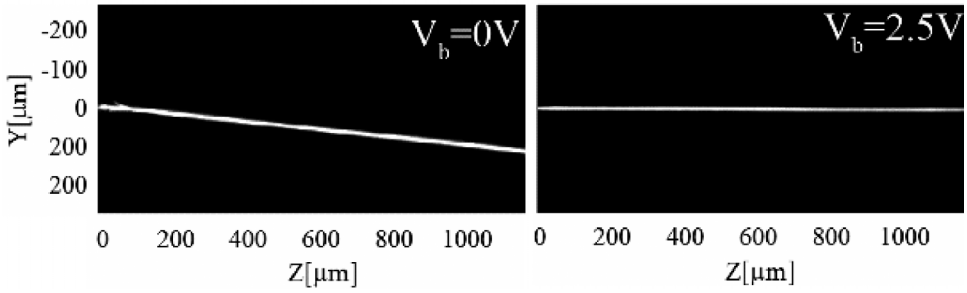

Figure 12. Photographs of a nematicon launched with a wave vector parallel to z in a planar cell with **n** in the plane yz at $\pi/4$ with respect to **E** // **y**. (Left) Propagation with a walk-off δ=7° in the yz plane and no applied voltage; (right) propagation at $\delta \approx 0°$ after a bias V=2.5V has reoriented **n** to be nearly parallel to x (ordinary configuration).

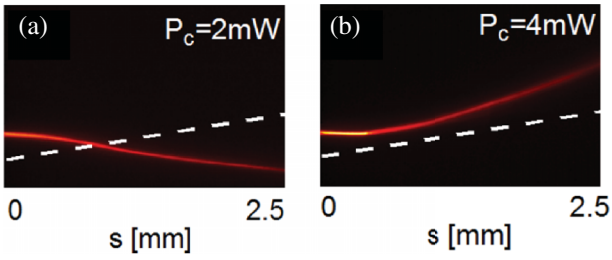

Figure 13. (a) Refraction of a nematicon through the double interface defined in a dye-doped NLC cell by an elongated beam of power P_c propagating across x and with major axis along the dashed line; (b) total internal reflection for a beam as in (a), but orthogonally polarized in order to induce a decrease in index. The coordinate s is taken along the Poynting vector.

Finally, a relatively wide region of higher index can be defined in an NLC cell by the use of electrodes and bias, effectively realising a waveguide or trapping potential for a nematicon with an initial transverse velocity. In analogy to a particle in a finite well, as the momentum associated to the soliton increases by means of its input power, the trapped beam eventually overcomes the potential barrier and leaves the waveguide. This was recently demonstrated in E7 and described with both a particle-like model and modulation theory (*57*, *58*).

4. Spatial solitons in twisted and chiral nematic liquid crystals

In twisted and chiral nematics, the molecular director is parallel to the surrounding glass plates (interfaces) and twisted within the layer thickness (Figure 14). Such an orientation is typically induced by the boundary conditions (in twisted nematics, TN) or by the chiral properties (cholesteric liquid crystals, ChNLC). For light polarised along y the refractive index varies across the sample thickness from ordinary value n_o in planes where $\theta = 0$ to extraordinary n_e in planes where $\theta = \pi/2$ (n_o and n_e are the ordinary and extraordinary refractive indices, respectively). A self-trapped light beam propagates in the thin film where the refractive index is the largest, close to n_e. Such film can be located in the middle of the layer (as in Figure 14(a), symmetric twist) or at one of its boundaries (as in Figure 14(b), asymmetric twist) (*59*). If the twist is periodic versus thickness (Figure 14(c)), a greater number of high index regions (films) occur throughout the liquid crystal.

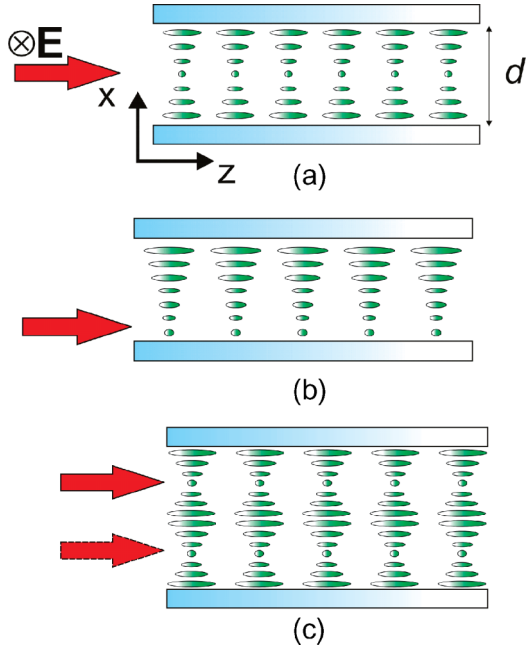

Figure 14. Configurations of non-homogeneous NLC layers: (a) symmetrically twisted, (b) asymmetrically twisted, (c) chiral, with the indication of two possible beam inputs.

In the investigated configurations a light beam propagates in the z-direction parallel to the glass plates. The beam is TE-polarised with the electric field vector $\mathbf{E} = \mathbf{y}E_y$ also parallel to the glass plates. The electric permittivity tensor in such a medium depends on the orientation angle θ and varies across the sample. In this case, the Maxwell equations for a monochromatic electromagnetic wave are (*60*, *61*)

$$\left[k_o^2\varepsilon_{yy} + \frac{\partial^2}{\partial x^2} + \frac{\partial^2}{\partial y^2}\frac{\varepsilon_{yy}}{\varepsilon_{xx}} + \frac{\partial^2}{\partial z^2} + \frac{\partial^2}{\partial y\partial z}\frac{\varepsilon_{yz}}{\varepsilon_{xx}}\right]E_y = \left[-k_o^2\varepsilon_{yz} - \frac{\partial^2}{\partial y^2}\frac{\varepsilon_{yz}}{\varepsilon_{xx}} - \frac{\partial^2}{\partial y\partial z}\left(\frac{\varepsilon_{zz}}{\varepsilon_{xx}} - 1\right)\right]E_z, \quad (5)$$

$$\left[k_o^2\varepsilon_{zz} + \frac{\partial^2}{\partial x^2} + \frac{\partial^2}{\partial y^2} + \frac{\partial^2}{\partial z^2}\frac{\varepsilon_{zz}}{\varepsilon_{xx}} + \frac{\partial^2}{\partial y\partial z}\frac{\varepsilon_{yz}}{\varepsilon_{xx}}\right]E_z = \left[-k_o^2\varepsilon_{yz} - \frac{\partial^2}{\partial z^2}\frac{\varepsilon_{yz}}{\varepsilon_{xx}} - \frac{\partial^2}{\partial y\partial z}\left(\frac{\varepsilon_{yy}}{\varepsilon_{xx}} - 1\right)\right]E_y, \quad (6)$$

with ε_{ab} the permittivity components and $k_0 = \omega/c$ the wave vector. Even if the beam is initially linearly polarised, during propagation all components of electric and magnetic fields should appear. However, only E_y and E_z are important for reorientation. Using the Euler–Lagrange equation for energy minimisation, the following partial differential equation is obtained:

$$K_{22}\left(\frac{\partial^2\theta}{\partial x^2}\right) + \frac{\varepsilon_0\Delta\varepsilon}{4}\left[\left(|E_z|^2 - |E_y|^2\right)\sin 2\theta + \left(E_y^*E_z + E_z^*E_y\right)\cos 2\theta\right] = 0 \quad (7)$$

where $\theta(x) = \theta_0 + 2\pi x/p$ is the initial orientation (without electric field) and p is the chirality pitch.

The description of propagation in a TN layer can be simplified by assuming that the beam profile along x is roughly constant, a hypothesis which is correct at some distance from the input, where the (self) guided mode is formed. In this assumption the fields are of the form

$$E_y = A(y,z)\varphi(x)\exp(i\omega t - ik_0Nz), \quad (8)$$

$$E_z = A(y,z)\phi(x)\exp(i\omega t - ik_0Nz), \quad (9)$$

where $\varphi(x)\exp(\mathrm{i}\omega t - \mathrm{i}k_0Nz)$ and $\phi(x)\exp(\mathrm{i}\omega t - \mathrm{i}k_0Nz)$ are components of the planar waveguide mode with an effective refractive index N. Taking $E_z << E_y$, the slowly varying amplitude A is ruled by

$$-2ik_0N\frac{\partial}{\partial z}A + \frac{\partial^2}{\partial y^2}\gamma_1 A - 2ik_0N\frac{\partial}{\partial y}\gamma_2 A + k_0^2\varepsilon_\perp\left(\gamma_1 - \gamma_1^{(0)}\right)A = 0; \quad (10)$$

the coefficients γ_1 and γ_2 depend on the orientation angle as

$$\gamma_1 = 1 + \frac{\Delta\varepsilon}{\varepsilon_\perp}\frac{\int\varphi^2\cos^2\theta\,\mathrm{d}x}{\int\varphi^2\mathrm{d}x},$$
$$\gamma_2 = \frac{\Delta\varepsilon}{2\varepsilon_\perp}\frac{\int\varphi^2\sin\theta\cos\theta\,\mathrm{d}x}{\int\varphi^2\mathrm{d}x}$$

and $\gamma_1{}^{(0)}$ is the value of γ_1 for the initial orientation. These coefficients are interpolated by

$$\gamma_1 = \gamma_1^{(0)} + \alpha_1\frac{|A|^2}{1 + |A/A_1|^2},$$
$$\gamma_2 = \gamma_2^{(0)} - \alpha_2\frac{|A|^2}{1 + |A/A_1|^2} \quad (12)$$

with the saturable amplitudes A_p as well as the constants $\gamma_p{}^{(0)}$ and α_p ($p = 1,2$) being calculated for a given NLC. γ_2 is connected with the walk-off of the light beam in asymmetric configurations. As the light intensity increases, γ_2 and the walk-off become smaller. This means that a change in light intensity affects the direction of beam propagation. γ_1 relates to non-linearity and is responsible for self-focusing and the creation of spatial solitons. The simplified equation predicts that a light beam gets self-trapped and changes walk-off with increasing optical intensity. In a symmetric configuration the walk-off vanishes and the light intensity only induces self-confinement.

Experimentally, it was demonstrated that twisted NLC can support spatial solitons for light powers of a few tens of milliwatt. In the asymmetric case the results also show a change in direction of propagation with increased excitation. Most experiments were carried out in a cell of thickness $d = 50$ μm filled with 6CHBT (4-trans-4'-n-hexyl-cyclohexyl-isothiocyanatobenzene) with refractive indices $n_o = 1.51$ and $n_e = 1.67$ (*62*, *63*). An Ar+ laser beam ($\lambda = 514$ nm) with initial waist of a few micrometers formed nematicons at powers close to 100 and 20 mW in the symmetric and asymmetric configurations, respectively (*64*, *65*). The solitary beam exhibited an invariant transverse distribution over a propagation distance more than 50 times the Rayleigh length (a few millimetres).

The relatively large power required to form nematicons in TN can be reduced with thickness d. However, if the thickness is too small, then thermal effects become more important and the self-focusing rather unstable. The problem can be eliminated by using chiral nematics with a small pitch instead of TN. Since the pitch defines molecular rotation by 2π, the thickness d in a TN geometry corresponds to a pitch $p = 4d$.

Nematicons in ChNLC are basically similar to those in TN; however, the former offers some new opportunities owing to the fact that the width of a guiding layer (in x) is not only determined by the sample (as in TN) but also by the chirality pitch. As a result, in ChNLC it is easier to define the thickness of a layer and – as a consequence – the proper non-linear strength. It is also possible to utilise multi-layers for the propagation of independent or interacting nematicons.

Spatial solitons in ChNLC were excited in the cell with pitch $p = 25$ μm (10 μm) at powers $P \approx 30$ mW (≈ 8 mW) (*66*, *67*). Typical results for a Ti:Sapphire ($\lambda = 790$ nm) laser beam with input waist of about 2 μm are presented in Figure 15(a) and (b). Nematicons were size invariant for about 2 mm (>80 times the Rayleigh length). Due to the finite thickness of each layer in ChNLC, only in a limited waist range self-focusing can exactly balance diffraction and give rise to self-trapped solitons. Moreover, by changing the vertical input position along x, it was possible to launch as many solitons as layers in the ChNLC structure, as visible in Figure 15(c), corresponding to the four layers of a cell about 50 μm thick and with a 25 μm pitch. The four nematicons could be injected independently and 10 to 12 μm apart from one another.

Finally, even in TN and ChNLC we verified that the solitary waveguide could confine different signals, particularly co-polarised low-power probe from a helium-neon laser ($\lambda = 632.8$nm).

5. Conclusions

Nematic liquid crystals, well-known materials with versatile properties and mature technology, are a perfect platform for the experimental investigation of light self-localisation and spatial optical solitons at milliwatt power levels and over millimetre distances. Their reorientational non-linearity, saturable and non-local, has

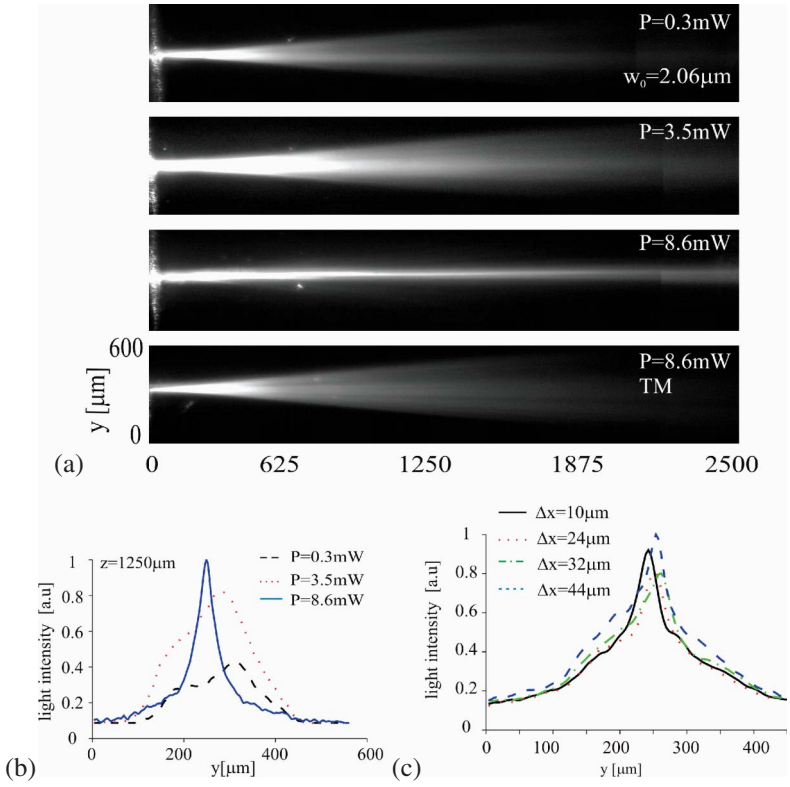

Figure 15. Experimental results on solitons in ChNLC: (a) light beam propagation for various input powers (marked on photos) and a centrally launched excitation; the last picture was taken for TM polarisation. (b) Beam intensity profiles at low and high powers, respectively, in $z = 1.25$ mm. (c) Nematicon cross-sections in different layers across the ChNLC and $z = 1$mm, as obtained by launching the beam in different vertical positions Δx.

enabled the demonstration of several soliton-based configurations for all-optical signal routing, switching, steering and readdressing. Moreover, a number of novel fundamental phenomena have been observed owing to their dielectric properties, non-locality, anisotropy, birefringence, extended transparency and electro-optic response. We anticipate a significant number of device and integrated microsystems demonstrations exploiting nematicons for signal processing in future generations of all-optical circuits.

Acknowledgements

We are grateful to various collaborators worldwide: R. Dąbrowski, M. Kaczmarek, I.C. Khoo, A.A. Minzoni, E. Nowinowski, S. Residori, M. Sierakowski, F. Simoni, N.F. Smyth, N. Tabiryan, C. Umeton and T.R. Wolinski. We are indebted to our students and associates over the years for the extensive contributions to the work reviewed hereby: A. Alberucci, C. Conti, A. Fratalocchi, K. Jaworowicz, M. Kwasny, U.A. Laudyn, A. Pasquazi, M. Peccianti, A. Piccardi and K.A. Rutkowska.

Work partially sponsored at UniRoma3 by the Air Force Office of Scientific Research, Air Force Material Command, USAF, under grant number FA8655-08-1-3045. The U.S Government is authorized to reproduce and distribute reprints for Governmental purpose notwithstanding any copyright notation thereon.

References

(1) de Gennes P.G. *The Physics of Liquid Crystals*; Clarendon Press, Oxford, 1974.
(2) Khoo I.C.; Wu N.T. *Optics and Nonlinear Optics of Liquid Crystals*; World Scientific Publishing: Singapore, 1993.
(3) Tabiryan N.V.; Sukhov A.V.; Zeldovich B.Ya. *Mol. Cryst. Liq. Cryst.* **1986**, *136*, 1–139.
(4) Simoni F. *Nonlinear Optical Properties of Liquid Crystals*; World Scientific Publishing: London, 1997.
(5) Assanto G.; Peccianti M.; Conti C. *Opt. Photon. News* **2003**, *14*, 44–48.
(6) Assanto G.; Peccianti M. *IEEE J. Quantum Electron.* **2003**, *39*, 13–21.
(7) Braun E.; Faucheux L.P.; Libchaber A. *Phys. Rev. A* **1993**, *48*, 611–622.
(8) Warenghem M.; Henninot J.F.; Abbate G. *Opt. Express* **1998**, *2*, 483–490.
(9) Derrien F.; Henninot J.F.; Warenghem M.; Abbate G. *J. Opt. A - Pure Appl. Opt.* **2000**, *2*, 332–337.
(10) Alberucci A.; Assanto G. *J. Opt. Soc. Am. B* **2007**, *24*, 2314–2320.
(11) Garcia-Reimbert C.; Minzoni A.A.; Smyth N.F.; Worthy A.L. *J. Opt. Soc. Am. B* **2006**, *23*, 2551–2558.
(12) Minzoni A.A.; Smyth N.F.; Worthy A.L. *J. Opt. Soc. Am. B* **2007**, *24*, 1549–1556.
(13) Karpierz M.A.; Sierakowski M.; Świłło M.; Woliński T.R. *Mol. Cryst. Liq. Cryst.* **1998**, *320*, 157–164.
(14) Karpierz M.A. *Phys Rev. E* **2002**, *66*, 036603.
(15) Fratalocchi A.; Assanto G.; Brzdąkiewicz K.A.; Karpierz M.A. *Opt. Lett.* **2004**, *29*, 1530–1532.
(16) Fratalocchi A.; Assanto G.; Brzdąkiewicz K.A.; Karpierz M.A. *Opt. Express* **2005**, 13, 1808–1813.
(17) Fratalocchi A.; Assanto G.; Brzdąkiewicz K.A.; Karpierz M.A. *Appl. Phys. Lett.* **2005**, *86*, 051109–051111.
(18) Lederer F.; Stegeman G.I.; Christodoulides D.N.; Assanto G.; Segev M.; Silberberg Y. *Phys. Rep.* **2008**, *463*, 1–126.
(19) Assanto G.; Fratalocchi A.; Peccianti M. *Opt. Express* **2007**, *15*, 5248–5259.
(20) Peccianti M.; Assanto G.; De Luca A.; Umeton C.; Khoo I.C. *Appl. Phys. Lett.* **2000**, *77*, 7–9.
(21) Conti C.; Peccianti M.; Assanto G. *Phys. Rev. Lett.* **2003**, *91*, 073901.
(22) Conti C.; Peccianti M.; Assanto G. *Phys. Rev. Lett.* **2004**, *92*, 113902.
(23) Snyder A.W.; Mitchell D.J. *Science* **1997**, *276*, 1538–1541.
(24) Peccianti M.; Fratalocchi A.; Assanto G. *Opt. Express* **2004**, *12*, 6524–6529.
(25) Peccianti M.; Assanto G. *Opt. Lett.* **2001**, *26*, 1690–1692.
(26) Alberucci A.; Assanto G.; Buccoliero D.; Desyatnikov A.S.; Marchant T.R.; Smyth N.F. *Phys. Rev. A* **2009**, *79*, 043816.
(27) Alberucci A.; Peccianti M.; Assanto G. *Opt. Lett.* **2007**, *32*, 2795–2797.
(28) Peccianti M.; Assanto G. *Opt. Lett.* **2001**, *26*, 1791–1793.
(29) Peccianti M.; Assanto G. *Phys. Rev. E* **2002**, *65*, 035603.
(30) Makris K.G.; Sarkissian H.; Christodoulides D.N.; Assanto G. *J. Opt. Soc. Am. B* **2005**, *22*, 1371–1377.
(31) Alberucci A.; Peccianti M.; Assanto G.; Dyadyusha A.; Kaczmarek M. *Phys. Rev. Lett.* **2006**, *97*, 153903.
(32) Assanto G.; Smyth N.F.; Worthy A.L. *Phys. Rev. A* **2008**, *78*, 013832.
(33) Peccianti M.; Brzdąkiewicz K.A.; Assanto G. *Opt. Lett.* **2002**, *27*, 1460–1462.
(34) Peccianti M.; C. Conti, Assanto G.; De Luca A.; Umeton C. *Appl. Phys. Lett.* **2002**, *81*, 3335–3337.
(35) Rasmussen P.D.; Bang O.; Królikowski W. *Phys. Rev. E* **2005**, *72*, 066611.
(36) Fratalocchi A.; Piccardi A.; Peccianti M.; Assanto G. *Opt. Lett.* **2007**, *32*, 1447–1449.
(37) Fratalocchi A.; Piccardi A.; Peccianti M.; Assanto G. *Phys. Rev. A* **2007**, *75*, 063835.
(38) Garcia-Reimbert C.; Minzoni A.A.; Marchant T.R.; Smyth N.F.; Worthy A.L. *Physica D* **2008**, *237*, 1088–1102.
(39) Pasquazi A.; Alberucci A.; Peccianti M.; Assanto G. *Appl. Phys. Lett.* **2005**, *87*, 261104–261106.
(40) Serak S.V.; Tabiryan N.V.; Peccianti M.; Assanto G. *IEEE Photon. Techn. Lett.* **2006**, *18*, 1287–1289.
(41) Peccianti M.; Conti C.; Assanto G. *Opt. Lett.* **2003**, *28*, 2231–2233.
(42) Peccianti M.; Conti C.; Assanto G. *Phys. Rev. E* **2003**, *68*, R025602.
(43) Assanto G.; Peccianti M.; Conti C. *IEEE J. Sel. Top. Quantum Electron.* **2004**, *10*, 862–869.
(44) Conti C.; Peccianti M.; Assanto G. *Phys. Rev. E* **2005**, *72*, 066614.
(45) Assanto G.; Marchant T.R.; Smyth N.F. *Phys. Rev. A* **2008**, *78*, 063808.
(46) Conti C.; Peccianti M.; Assanto G. *Opt. Lett.* **2006**, *31*, 2030–2032.

(47) Conti C. *Phys. Rev. E* **2005**, *72*, 066620.
(48) Peccianti M.; Conti C.; Assanto G.; De Luca A.; Umeton C. *Nature* **2004**, *432*, 733–737.
(49) Alberucci A.; Peccianti M.; Assanto G.; Coschignano G.; De Luca A.; Umeton C. *Opt. Lett.* **2005**, *30*, 1381–1383.
(50) Piccardi A.; Bortolozzo U.; Residori S.; Assanto G. *Opt. Lett.* **2009**, *34*, 737–739.
(51) Peccianti M.; Dyadyusha A.; Kaczmarek M.; Assanto G. *Nat. Phys*. **2006**, *2*, 737–741.
(52) Peccianti M.; Assanto G.; Dyadyusha A.; Kaczmarek M. *Phys. Rev. Lett.* **2007**, *98*, 113902.
(53) Peccianti M.; Conti C.; Assanto G. *Opt. Lett*. **2005**, *30*, 415–417.
(54) Peccianti M.; Assanto G.; Dyadyusha A.; Kaczmarek M. *Opt. Lett.* **2007**, *32*, 271–273.
(55) Piccardi A.; Assanto G.; Lucchetti L.; Simoni F. *Appl. Phys. Lett.* **2008**, *93*, 171104.
(56) Peccianti M.; Assanto G. *Opt. Express* **2007**, *15*, 8021–8028.
(57) Peccianti M.; Dyadyusha A.; Kaczmarek M.; Assanto G. *Phys. Rev. Lett.* **2008**, *101*, 153902.
(58) Assanto G.; Minzoni A.A.; Peccianti M.; Smyth N.F. *Phys. Rev. A* **2009**, *79*, 033837.
(59) Karpierz M.A. *Acta Phys. Pol. A* **2001**, *99*, 161–173.
(60) Karpierz M.A.; Sierakowski M.; Woliński T.R. *Mol. Cryst. Liq. Cryst.* **2002**, *375*, 313–320.
(61) Karpierz M.A.; Brzdąkiewicz K.A.; Nguyen Q.V. *Acta Phys. Pol.* A **2003**, *103*, 169–175.
(62) Baran J.; Raszewski Z.; Dąbrowski R.; Kędzierski J.; Rutkowska J. *Mol. Cryst. Liq. Cryst.* **1985**, *123*, 237–242.
(63) Dąbrowski R.; Dziaduszek J.; Szczuciński T. *Mol. Cryst. Liq. Cryst.* **1985**, *124*, 241–246.
(64) Jaworowicz K.; Brzdąkiewicz K.A.; Karpierz M.A.; Sierakowski M. *Mol. Cryst. Liq. Cryst*. **2006**, *453*, 301–307.
(65) Laudyn U.A.; Kwaśny M.; Jaworowicz K.; Rutkowska K.A.; Karpierz M.A.; Assanto G. *Photon. Lett. Pol.* **2009**, *1*, 7–9.
(66) Laudyn U.A.; Jaworowicz K.; Karpierz M.A. *Mol. Cryst. Liq. Cryst.* **2008**, *489*, 214–221.
(67) Laudyn U.A.; Kwaśny M.; Karpierz M.A. *Appl. Phys. Lett.* **2009**, *94*, 091110–091112.